Direct modulation and bandwitdh measurement of terahertz quantum cascade laser

Yoann Petitjean, Fabien Destic, Stefano Barbieri, Carlo Sirtori, Jean-Claude Mollier

Direct modulation and bandwitdh measurement of terahertz quantum cascade laser

Yoann Petitjean[a], Fabien Destic[a], Stefano Barbieri[c], Carlo Sirtori[c], and Jean-Claude Mollier[a,b]

[a]Institut Supérieur de l'Aéronautique et de l'Espace, 10 Av. Edouard Belin – 31055 Toulouse
[b]ONERA, 2 Av. Edouard Belin – 31055 Toulouse, France
[c]Université Paris 7 Denis Diderot – Laboratoire MPQ – 75205 Paris, France

ABSTRACT

The authors present a home made cryogenic electro-optical probe station allowing the direct modulation of quantum cascade lasers up to 40GHz. Based on a QMC cryostat, it should make the QCL bandwidth measure possible and then help answering questions about the modulation possibilities of such a kind of laser. The experimental results will be compared to simulation bandwidth prediction based on a complete set of rate equations describing the dynamic behavior of the laser. Bandwidth will be then linked to the different intrinsic and structural parameters.

Keywords: Bandwidth measurement, Quantum Cascade Laser, Modulation, Modelling

1. INTRODUCTION

This paper aims at proposing a theoretical description of small signal modulation of Quantum Cascade Lasers (QCL). Their invention in 1994 by Faist, Capasso *et al.*[1] brought a powerful and compact solid source of far infrared radiation. Since then, their performances have continuously improved. Terahertz QCL working above liquid nitrogen temperature,[2,3] and even at room temperature by intracavity difference-frequency generation, have been reported.[4] Their spectral range is now extending from the mid-infrared down to 1.2 THz.[5] Due to the novel properties and unique interaction with many materials, the terahertz radiation has become a topic of active research for the past few years, and is still a going concern.[6,7] Among the large possibilities of applications, free space short range communications have been studied[8,9] because of the Wi-Fi capabilities of terahertz waves and QCL large supposed bandwidth modulation.[10] QCL-based local oscillators are also attractive for radioastronomy applications[11] thanks to their high spectral purity, adequate output power and good stability. Modeling the behavior of QCLs is therefore an important step toward the prediction of performances of such semi-conductor sources. Microscopic modelings have proved to be relevant in predicting and analyzing quantum device carrier dynamics and have largely participate to their design improvement.[12,13]

However, hereinbefore mentioned applications need a more global consideration of the optoelectronic system, and the establishment of a small signal equivalent circuit appears to be useful with this end in view. That is the final purpose of the theory presented in this paper. Indeed, theoretical study of electro-optical behavior, associated with the electrical ports S-parameters of a QCL should create a link between experimental measurements and intrinsic parameters values of the laser diode, and a better prediction of embedded device behavior. This method has proved to be apposite for many kinds of semiconductor lasers used in such applications. Macroscopic theoretical modeling of the QCL dynamic are easily usable: the set of rate equations governing the number of photons in the cavity and of electrons on the different possible states, along with their different lifetimes are sufficient.

Considering the full rate equations system,[14] a numerical simulation is firstly established. It leads to modulation bandwidth up to a few dozens of gigahertz. Then, an analytical calculation is made to propose a transfer function that is simplified next, in order to study its dependence as a function of various parameters like lifetimes and number of periods.

Further author information: (Send correspondence to Yoann Petitjean)
Yoann Petitjean: E-mail: yoann.petitjean@isae.fr
Fabien Destic: E-mail: fabien.destic@isae.fr

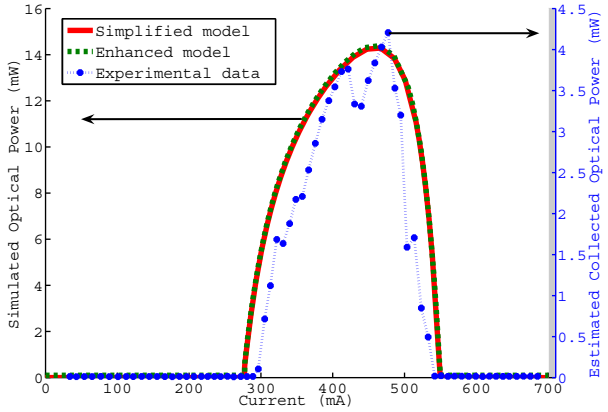

Figure 1. Optical power versus current of a 30-periods QCL (dotted line : experimental data, solid line : simplified model and dashed line : enhanced model)[16]

2. SIMPLIFIED MODEL

2.1 Rate Equations

The simplified rate equations are based on a three-level classical scheme which leads to a 3 equations-system (2 for electrons on the two levels involved in the laser transition and 1 for photons). For a QCL of N_p periods, these equations are written as follows (Eq.(1) to (3))[15] :

$$\frac{\partial N_3}{\partial t} = \eta \frac{I}{q} - \frac{N_3}{\tau_3} - G\,(N_3 - N_2)\,P \tag{1}$$

$$\frac{\partial N_2}{\partial t} = \frac{N_3}{\tau_{32}} - \frac{N_2}{\tau_2} + G\,(N_3 - N_2)\,P \tag{2}$$

$$\frac{\partial P}{\partial t} = N_p\,G\,(N_3 - N_2)\,P - \frac{P}{\tau_p} + \beta\frac{N_3}{\tau_{sp}} \tag{3}$$

where N_i is the number of electrons in the i^{th} level, P the number of photons, G the optical gain, τ_{32} the non-radiative scattering time, τ_i the electron lifetime in level i, and τ_p the photon lifetime. τ_{sp} is the spontaneous emission lifetime.

2.2 Benefits and inaccuracies of this model

These rate equations well describe the static behavior of quantum cascade lasers, as they lead to the same result than the full system as illustrated in fig.(1). The much more simple calculation needed for this model allows quite simple analytical results. Moreover, as other macroscopic theories that allow to deduce a small signal equivalent circuit, helpful for optoelectronic applications like direct intensity modulation communications, this modeling is very valuable.

However, this simplified modeling leads to a root-squared-law increase of the bandwidth with the number of periods. It is not a quite intuitive result. Indeed, the extraction time of the electrons to pass through the different periods is not taken into account. We can spontaneously think that this extraction time could decrease the small signal bandwidth of the QCL. That will be discussed further. Because of this simplification, small signal equivalent circuits deduced from this set of equations might lead to inaccuracies.

3. FULL RATE EQUATIONS

The previous set of rate equations is actually deduced from a more complex one. In order to take into account the extraction time of the electrons to pass from the fundamental level of the i^{th} period to the excited one of the $i+1^{th}$ period, one more equation has to be reintegrated. The rate equations are consequently based on a three-level scheme with 4 equations (one for each of the three levels of the electrons and one for the photons).[14] This so called full rate equation system is given by Eq.(4) to Eq.(7) :

$$\frac{\partial N_3^{(j)}}{\partial t} = \eta \frac{{I_{in}}^{(j)}}{q} - \frac{N_3^{(j)}}{\tau_3} - G^{(j)} (N_3^{(j)} - N_2^{(j)}) P \tag{4}$$

$$\frac{\partial N_2^{(j)}}{\partial t} = \frac{N_3^{(j)}}{\tau_{32}} - \frac{N_2^{(j)}}{\tau_2} + G^{(j)} (N_3^{(j)} - N_2^{(j)}) P \tag{5}$$

$$\frac{\partial N_1^{(j)}}{\partial t} = \frac{N_3^{(j)}}{\tau_{31}} - \frac{N_2^{(j)}}{\tau_{21}} - \frac{{I_{out}}^{(j)}}{q} \tag{6}$$

$$\frac{\partial P}{\partial t} = \sum_{j=1}^{N_p} G^{(j)} (N_3^{(j)} - N_2^{(j)}) P + n_{sp} \frac{N_3^{(j)} - N_2^{(j)}}{\tau_{sp}} - \frac{P}{\tau_p} \tag{7}$$

where N_i is the number of electrons in the i^{th} level, P the number of photons in the cavity, $G^{(j)}$ the optical gain of the j^{th} period, τ_i the electron lifetime in level i, and τ_p the photon lifetime. τ_{31}, τ_{32}, τ_{21} are the non radiative scattering times that are due to LO-phonon emission between the corresponding levels. n_{sp} is the spontaneous emission coefficient and τ_{sp} the radiative spontaneous relaxation time. $I_{in}^{(j)}$ and $I_{out}^{(j)}$ are respectively the input and output currents of the j^{th} period. For the first period, $I_{in}^{(1)}$ comes down to the input current of the QCL.

Moreover, in order to describe the cascade scheme of the QCL, since the input current of the j^{th} period is the output current of the $(j-1)^{th}$ period, these currents can be linked to a number of electrons extracted from the lower level of the $(j-1)^{th}$ period and injected on the upper level of the j^{th} period. Then, the output current of the j^{th} period is the rate of electrons leaving the level (1) given by Eq.(8) and the input current of the j^{th} period is the rate of electrons arriving on the level (3) from the level (1) of the previous period, given by Eq.(8).

$$\frac{{I_{out}}^{(j)}}{q} = \frac{N_1^{(j)}}{\tau_{out}} \quad , \quad \frac{{I_{in}}^{(j)}}{q} = \frac{N_1^{(j-1)}}{\tau_{out}} \tag{8}$$

4. ANALYTICAL RESOLUTION

4.1 Hypotheses

The analytical resolution of the full rate equation is quite difficult for the time being. Consequently, one has to assume some simplifying hypotheses. First of all, the gain is supposed constant in the different periods. However, it could be an interesting job to focus on the spatial non-uniformity of the gain to describe furthermore the reality of the static and dynamic behavior. Secondly, the spontaneous emission term in the last equation is neglected as compared with the stimulated one. It is a well-known and quite correct assumption as soon as the laser is biased well above threshold. Last assumption, the η coefficient standing for the non-perfect injection of the electrons on the excited level will be supposed equal to 1. The value of this parameter has mainly an impact on the static behavior.

Table 1. Device parameters used in numerical simulations (unless stated otherwise) (from[14, 15, 17, 18])

Parameter	Value
Number of periods N_p	30
Confinement factor Γ	0.27
Cavity losses α_i	24cm^{-1}
Gain G	5.3×10^4 s^{-1}
Equilibrium population inversion ΔN_0	10^5
Equilibrium photon number P_0 @$I_0 = 450mA$	2.3×10^8
τ_{out}	0.5 ps
τ_2	0.3 ps
τ_3	1.1 ps
τ_{31}	2.4 ps
τ_{32}	2 ps
τ_p	3.7 ps
τ_{sp}	7 ns

4.2 Linearized equations

From the rate equations above, a small perturbation method will be used to linearize them. Thus, the number of photons $P(t)$ will be the sum of the steady-state value P_0 and a small variation $p(t)$ around P_0. In the same way, the different numbers of electrons $N_i^{(j)}(t)$ in each level will be the sum of a steady-state term ${N_{i0}}^{(j)}$ and a perturbation one $n_i^{(j)}(t)$.

This method, associated with the previous hypotheses leads to a linearized set of four rate equations, that can be written in the Laplace domain (s will be the Laplace variable and $X(s)$ the Laplace transform of $x(t)$).

$$\left(s + \frac{1}{\tau_3} + G\,P_0\right) N_3^{(j)}(s) = \frac{N_1^{(j-1)}(s)}{\tau_{out}} + G\,P_0\,N_2^{(j)}(s) - G\,\Delta N_0\,P(s) \quad (9)$$

$$\left(s + \frac{1}{\tau_2}\right) N_2^{(j)}(s) = \frac{N_3^{(j)}(s)}{\tau_{32}} + G\,P_0\,N_3^{(j)}(s) + G\,\Delta N_0\,P(s) \quad (10)$$

$$\left(s + \frac{1}{\tau_1}\right) N_1^{(j)}(s) = \frac{N_3^{(j)}(s)}{\tau_{31}} + \frac{N_2^{(j)}(s)}{\tau_{21}} \quad (11)$$

$$\left(s + \frac{1}{\tau_p} - G\,N_p\,\Delta N_0\right) P(s) = -\,G\,P_0 \sum_{j=1}^{N_p} \left(N_3^{(j)}(s) - N_2^{(j)}(s)\right) \quad (12)$$

where $\Delta N_0 = {N_{30}}^{(j)} - {N_{20}}^{(j)}$ is a constant for the different period j and it is actually the case in the simulations.

This recurrent state system, associated with Eq. (12), can be described by a more complex global state system allowing us to link the optical power P_{opt}(s) to I(s).

4.3 Analytic Transfer Function Calculation

Then, the small signal electro-optical transfer function $H(s)$ is given by Eq.(13) :

$$H(s) = \frac{P_{opt}(s)}{I(s)} = \alpha_m \frac{c}{n_g} \frac{h\,\nu}{q}\,k\,\frac{(-1)^{(3N_p+2)}\,Cof_{1,Np}}{det\,([\Omega])} \quad (13)$$

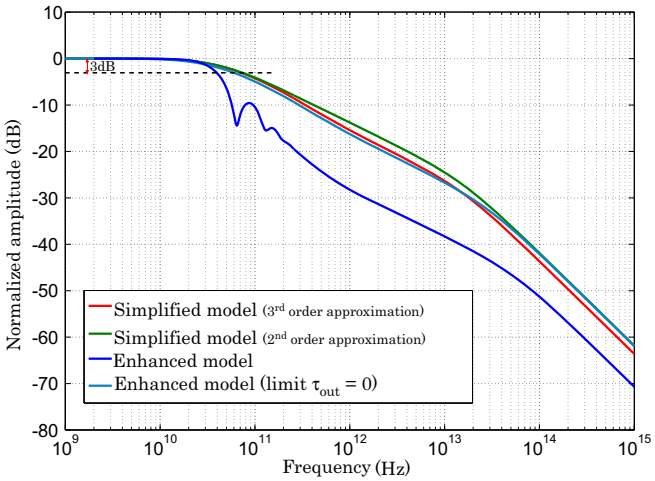

Figure 2. Comparison between full numerical simulation and linearized state system of a 30-periods QCL.

with

$$det\left([\Omega]\right) = (-1)^{(3N_p+1)}\sigma\left(\sum_{k=0}^{N_p-1}(-d)^k\ \left(Cof_{1,N_p-k}\ +\ Cof_{2,N_p-k}\right)\right) + \delta\, d^{N_p} \tag{14}$$

$$Cof_{1,k} = -Cof_{1,1}\sum_{i=0}^{k-1}\left(a_1^{k-i-1}\, d^i\right) \tag{15}$$

$$Cof_{2,k} = (-1)^{3N_p}\, a_2\, Cof_{1,k-1}\ +\ Cof_{2,1}\, d^{k-1} \tag{16}$$

$$a_1 = -\frac{k\,\sigma}{\tau_{out}}\left(\alpha_{21}\,\alpha_{32}\ -\ \alpha_{22}\,\alpha_{31}\right)\ ,\ a_2\ =\ -\frac{k\,\sigma}{\tau_{out}}\left(\alpha_{11}\,\alpha_{32}\ -\ \alpha_{12}\,\alpha_{31}\right) \tag{17}$$

$$d = det\left([\mathbb{A}]\right)\ ,\ \delta\ =\ k\left(s + N_p\, G\,\Delta N_0 + \frac{1}{\tau_p}\right) \tag{18}$$

$$Cof_{1,1} = \sigma\,\alpha_{33}\left(\alpha_{21}+\alpha_{22}\right)\ ,\ Cof_{2,1}\ =\ \sigma\,\alpha_{33}\left(\alpha_{11}+\alpha_{12}\right) \tag{19}$$

$$[\mathbb{A}] = k\begin{bmatrix} s+\frac{1}{\tau_3}+G\,P_0 & -G\,P_0 & 0 \\ -\frac{1}{\tau_{32}}-G\,P_0 & s+\frac{1}{\tau_2}+G\,P_0 & 0 \\ -\frac{1}{\tau_{31}} & -\frac{1}{\tau_{32}} & s+\frac{1}{\tau_{out}} \end{bmatrix} = \begin{bmatrix} \alpha_{11} & \alpha_{12} & 0 \\ \alpha_{21} & \alpha_{22} & 0 \\ \alpha_{31} & \alpha_{32} & \alpha_{33} \end{bmatrix} \tag{20}$$

where $k\ =\ \frac{1}{G\,P_0} \approx 8.2\times10^{-14}$ is a scale factor avoiding overflow during numerical computation.

The higher degree Laplace terms 's' of this transfer function is $Cof_{1,1}\, d^{N_p-1}$ for the numerator and $\delta\, d^{N_p}$ for the denominator. They respectively correspond to an s^{3N_p-1} term over an s^{3N_p+1}. Indeed, the higher degree term of $d = det\left([\mathbb{A}]\right)$ is s^3, the higher one of δ is s, and the higher one of $Cof_{1,1}$ is s^2. Therefore, the calculation leads to a globally second-order transfer function.

5. INVESTIGATION ON THE TURN-ON DELAY

5.1 Results based on the simplest model

These results are extracted from reference 19 and are presented here, for comparison.

- Rise time of the population inversion

The time $t_{\Delta N_{th}}$ taken by the electron population inversion to reach its threshold value is defined by :

$$\frac{\xi_3\, e^{-\frac{t_{\Delta N_{th}}}{\tau_3}} \;-\; \xi_2\, e^{-\frac{t_{\Delta N_{th}}}{\tau_2}}}{\xi_3 \;-\; \xi_2} \;=\; 1 \;-\; \frac{I_{th}}{I} \tag{21}$$

with :

$$\xi_3 = 1 + \frac{\tau_2}{\tau_{32}} \cdot \frac{\tau_3}{\tau_2 - \tau_3} \quad , \quad \xi_2 = \frac{\tau_2}{\tau_{32}} \cdot \frac{\tau_2}{\tau_2 - \tau_3} \tag{22}$$

- Rise time of the photons

The rise time of the photon number to reach 10% of the final value is :

$$t_{10\%S_0} = \frac{\tau_p}{\frac{I_0}{I_{th}} - 1}\, \ln\left[1 + \left(\frac{1}{I_{th}} - \frac{1}{I_0}\right)\, \frac{q\,\tau_{sp}}{\beta\,\tau_p\,\tau_3}\, \frac{S_0}{10}\right] \tag{23}$$

- Turn-on Delay for one period

Finaly, the Turn-on Delay (ToD) is the sum of the two previous contributions :

$$\Delta t \;=\; t_{\Delta N_{th}} \;+\; \frac{\tau_p}{\frac{I_0}{I_{th}} - 1}\, \ln\left[1 + \left(\frac{1}{I_{th}} - \frac{1}{I_0}\right)\, \frac{q\,\tau_{sp}}{\beta\,\tau_p\,\tau_3}\, \frac{P_0}{10}\right] \tag{24}$$

5.2 *Enhanced model*

The previous study, based on the simplified rate equations does not take into account the time needed by electrons to go from one period to the next one. We are going to analyse what happens when equations (4) to (7) are used to derive the ToD.

Assuming the photon number is still null, we compute the inversion population. Then, the relations linking $N_3^{(j)}(s)$ and $N_2^{(j)}(s)$ to $N_1^{(j-1)}(s)$ are the following:

$$\begin{aligned} N_1^{(j)}(s) \;&=\; T(s) \cdot N_1^{(j-1)}(s) \\ N_3^{(j)}(s) \;&=\; \frac{\frac{1}{\tau_{out}}}{p + \frac{1}{\tau_3}}\, N_1^{(j-1)}(s) \\ N_2^{(j)}(s) \;&=\; \frac{\frac{1}{\tau_{32}\,\tau_{out}}}{\left(s + \frac{1}{\tau_3}\right)\left(s + \frac{1}{\tau_2}\right)}\, N_1^{(j-1)}(s) \end{aligned} \tag{25}$$

with :

$$T(s) \;= \frac{1}{\tau_{out}}\, \frac{\frac{1}{\tau_{32}\,\tau_2} + \frac{1}{\tau_{31}}\left(s + \frac{1}{\tau_2}\right)}{\left(s + \frac{1}{\tau_3}\right)\left(s + \frac{1}{\tau_2}\right)\left(s + \frac{1}{\tau_{out}}\right)} \tag{26}$$

We can then obtain the total population inversion given by :

$$\begin{aligned}\Delta N_{tot}(s) &= \sum_{j=1}^{N_p} \Delta N^{(j)}(s) = \sum_{j=1}^{N_p} \left(N_3^{(j)}(s) - N_2^{(j)}(s) \right) \\ &= \left(\frac{1}{p + \frac{1}{\tau_3}} - \frac{\frac{1}{\tau_{32}}}{\left(s + \frac{1}{\tau_3}\right)\left(s + \frac{1}{\tau_2}\right)} \right) \frac{1 - T(s)^{N_p}}{1 - T(s)} \cdot \frac{I(s)}{q} = G(s, N_p) \cdot I(s)\end{aligned} \tag{27}$$

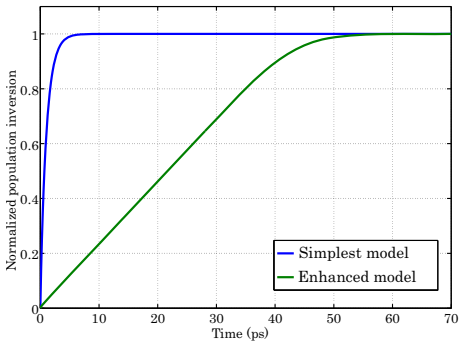

(a) Comparison between the temporal evolution of the populaiton inversion calculated from the simplest and the enhanced model.

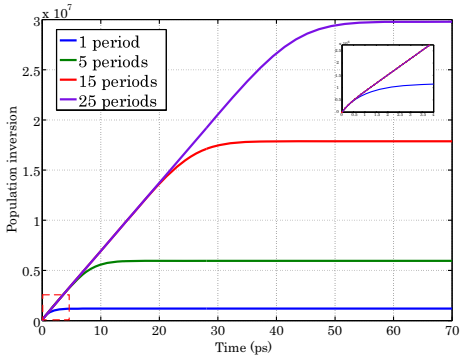

(b) Temporal evolution of the population inversion for different number of periods. The inset represents a zoom of the area inside the dashed red rectangular box.

Figure 3. legende

Whatever the number of periods is, the slope χ of the linear part of the temporal evolution of the population inversion is constant. Then, the time taken to reach the final value ΔN_{0tot} of the population inversion is given by $\frac{\Delta N_{0tot}}{\chi}$

with :

$$\begin{aligned}\chi &= \lim_{s \to 0} s^2 \left(\frac{1}{s + \frac{1}{\tau_3}} - \frac{\frac{1}{\tau_{32}}}{\left(s + \frac{1}{\tau_3}\right)\left(s + \frac{1}{\tau_2}\right)} \right) \frac{1}{1 - T(s)} \cdot \frac{I(s)}{q} \\ &= \frac{\tau_{31}\,\tau_{32} - \tau_2\,\tau_{31}}{\tau_{out}\left(\tau_{31} + \tau_{32}\right) + \tau_{31}\left(\tau_2 + \tau_{32}\right)} \cdot \frac{I_0}{q}\end{aligned} \tag{28}$$

The photon number rise time can be neglected here because the photon number starts to increase during the establishement of the population inversion. In conclusion, the ToD is equal to $t_{\Delta N_{tot}}$.

$$\begin{aligned}t_{\Delta N_{tot}} &= t_{\Delta N_{th}} + \frac{\Delta N_{0tot}}{\chi} \\ &= t_{\Delta N_{th}} + \tau_3 \left(1 - \frac{\tau_2}{\tau_{32}}\right) \frac{\tau_{out}\left(\tau_{31} + \tau_{32}\right) + \tau_{31}\left(\tau_2 + \tau_{32}\right)}{\tau_{31}\,\tau_{32} - \tau_2\,\tau_{31}}\end{aligned} \tag{29}$$

6. EXPERIMENTAL SETUP

In order to experimentally establish the bandwidth of QCLs, a test bench has been developed. It consists in a home-made electro-optical probe station, based on a TK1813 QMC Instruments Ltd. cryostat. A Cascade

Microtech microwave probe and special feedthrough allow applying both the bias and modulation current up to 40 GHz. This probe is driven by a three-axis micrometer stage. Two others three-axis micrometric stages drive two optical 1,55 μm focalizers(see fig.(4)). Indeed, since no fast enough THz detector is currently available, an up-conversion toward telecoms wavelength has been planned.[20,21] Because of the second order non-linear susceptibility χ_2 of GaAs, the whole THz spectra with microwave modulation sidebands is shifted on both sides of the telecom wavelength line. Modulation frequencies as high as 13 GHz[22] and more recently 24GHz[23] have been achieved with this technique. This test bench will allow us to have access to the Bode diagram magnitude of a QCL to validate our modeling. Based on this theory, work is in progress to propose small signal equivalent circuit of QCL, helpful for direct modulation applications. The different elements of the circuit are then linked to intrinsic parameters and optimization of the QCL in accordance with the application is possible. It is also an efficient method to get access to the intrinsic parameters of the laser chip under test and to evaluate the device features, in the same way as the technique used for more conventional lasers like VCSELs.[24]

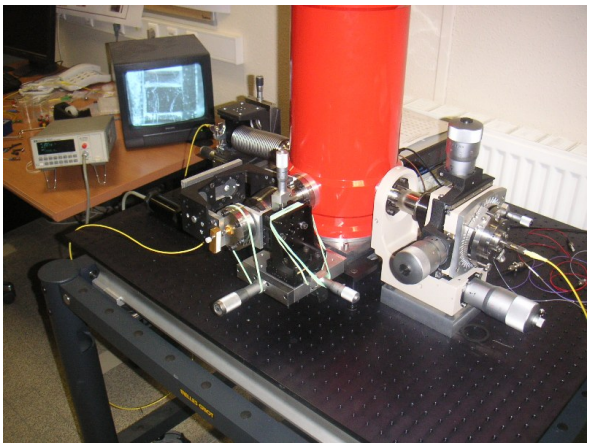

(a) Presentation of the experimental setup with the three-axis micrometric stages. An binocular microscope with camera allows us to see inside the cryostat, as we can catch sight of the QCL chip on the monitor

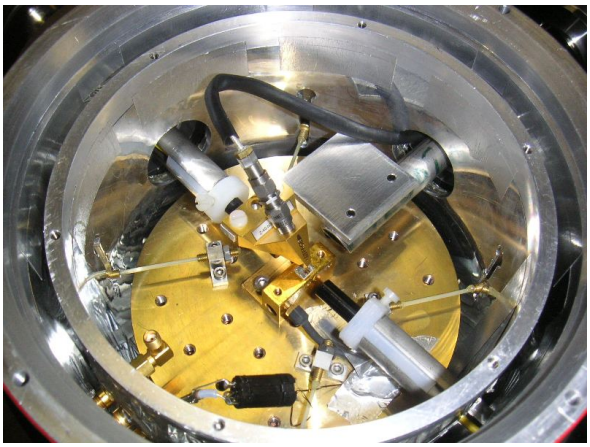

(b) View of the inside of the modified QMC cryostat. We can see the two optical focalizer and the microwave probe.

Figure 4. Photos of the experimental setup

7. CONCLUSION

A simplified transfer function, taking account of QCL cascade scheme architecture has been presented. The time constant variations of this transfer function have been pointed out and lead to a dependence of the direct modulation bandwidth with the number of periods and the electron extraction time. Numerical functions have been proposed, they could be useful for predicting the dynamic QCL performances. Further work and experiments are in progress to experimentally prove these dependences.

REFERENCES

1. J. Faist, F. Capasso, D. L. Sivco, C. Sirtori, A. L. Hutchinson, and A. Y. Cho, "Quantum cascade laser," *Science* **264**, April 1994.
2. G. Scalari, L. Ajili, J. Faist, H. Beere, E. Linfield, D. Ritchie, and G. Davies, "Far-infrared bound-to-continuum quantum-cascade lasers operating up to 90 k," *Applied Physic Letters* **82**, May 2003.
3. S. Kumar, Q. Hu, and J. L. Reno, "186 k operation of terahertz quantum-cascade lasers based on a diagonal design," *Applied Physic Letters* **94**, April 2009.
4. M. A. Belkin, F. Capasso, F. Xie, A. Belyanin, M. Fischer, A. Wittmann, and J. Faist, "Room temperature terahertz quantum cascade laser source based on intracavity difference-frequency generation," *Applied Physic Letters* **92**, May 2008.

5. C. Walther, M. Fischer, G. Scalari, R. Terazzi, N. Hoyler, and J. Faist, "Quantum cascade lasers operating from 1.2 to 1.6 thz," *Applied Physic Letters* **91**, September 2007.
6. P. H. Siegel, "Terahertz technology," *IEEE Transaction on Microwave Theory and Technique* **50**, March 2002.
7. D. Saeedkia and S. Safavi-Naeini, "Terahertz photonics: Optoelectronic techniques for generation and detection of terahertz waves," *IEEE Journal of lightwave technology* **26**, August 2008.
8. F. Capasso, R. Paiella, R. Martini, R. Colombelli, C. Gmachl, T. L. Myers, M. S. Taubman, R. M.Williams, C. G. Bethea, K. Unterrainer, H. Y. Hwang, D. L. Sivco, A. Y. Cho, A. M. Sergent, H. C. Liu, and E. A. Whittaker, "Quantum cascade lasers: Ultrahigh-speed operation, optical wireless communication, narrow linewidth, and far-infrared emission," *IEEE Journal of Quantum Electronics* **38**, June 2002.
9. R. Piesiewicz, M. Islam, M. Koch, and T. Kurner, "Towards Short-Range Terahertz Communication Systems: Basic Considerations," in *ICECom*, 2005.
10. N. Mustapha, L. Pesquera, C. Y. L. Cheung, and K. A. Shore, "Terahertz bandwidth prediction for amplitude modulation response of unipolar intersubband semiconductor lasers," *IEEE Photonics Technology Letters* **11**, May 2005.
11. J. R. Gao, J. N. Hovenier, Z. Q. Yang, J. J. A. Baselmans, A. Baryshev, M. Hajenius, T. M. Klapwijk, A. J. L. Adam, and T. O. Klaassen, "Terahertz heterodyne receiver based on a quantum cascade laser and a superconducting bolometer," *Applied Physic Letters* **86**, June 2005.
12. R. C. Iotti and F. Rossi, "Microscopic modelling of opto-electronic quantum devices: A predictive simulation tool," *Journal of Computational Electronics* **2**, December 2004.
13. R. C. Iotti and F. Rossi, "Microscopic modelling of semiconductor-based quantum devices: a predictive simulation strategy," *Physica status solidi B* **238**, July 2003.
14. F. Rana and R. J. Ram, "Current noise and photon noise in quantum cascade lasers," *Physical Review B* **65**, March 2002.
15. M. K. Haldar, "A simplified analysis of direct intensity modulation of quantum cascade laser," *IEEE Journal of Quantum Electronics* **41**, November 2005.
16. Y. Petitjean, F. Destic, and J.-C. Mollier, "Bandwidth simulation and measurement of Terahertz Quantum Cascade Laser," in *IRMMW-THz*, 2009.
17. J. Faist, L. Ajili, G. Scalari, M. Giovannini, M. Beck, M. Rochat, H. E. Beere, A. G. Davies, E. H. Linfield, and D. A. Ritchie, "Terahertz quantum cascade laser," *The Royal Society* , December 2003.
18. C. Sirtori, "Quantum cascade laser : fundamentals and performances," in *EDP sciences*, 2002.
19. A. Hamadou, S. Lamari, and J.-L. Thobel, "Dynamic modeling of a midinfrared quantum cascade laser," *Journal of Applied Physics* **105**, May 2009.
20. S. S. Dhillon, C. Sirtori, S. Barbieri, A. de Rossi, M. Calligaro, H. E. Beere, and D. A. Ritchie, "Thz sideband generation at telecom wavelengths in a gaas-based quantum cascade laser," *Applied Physic Letters* **87**, March 2005.
21. S. S. Dhillon, C. Sirtori, J. Alton, S. Barbieri, A. de Rossi, H. E. Beere, and D. A. Ritchie, "Terahertz transfer onto a telecom optical carrier," *Nature Photonics* **1**, July 2007.
22. S. Barbieri, W. Maineult, S. S. Dhillon, C. Sirtori, J. Alton, N. Breuil, H. E. Beere, and D. A. Ritchie, "13 ghz direct modulation of terahertz quantum cascade lasers," *Applied Physic Letters* **91**, August 2007.
23. W. Maineult, L. Ding, P. Gellie, P. Filloux, C. Sirtori, S. Barbieri, T. Akalin, J.-F. Lampin, I. Sagnes, H. E. Beere, and D. A. Ritchie, "Microwave modulation of terahertz quantum cascade laser : a transmission-line approach," *Applied Physic Letters* **96**, January 2010.
24. A. Bacou, A. Hayat, V. Iakovlev, A. Syrbu, A. Rissons, J.-C. Mollier, and E. Kapon, "Electrical modeling of long-wavelength vcsels for intrinsic parameters extraction," *IEEE Journal of Quantum Electronics* **46**, March 2010.